GCAGS JOURNAL
A Publication of the Gulf Coast Association of Geological Societies
www.gcags.org

Cyclicity of Carbonate Shoaling Sequences of the Lower Cretaceous Pettet Formation, Rusk County, East Texas

Kelly E. Hattori and Robert G. Loucks

Bureau of Economic Geology, University of Texas at Austin, P.O. Box X, Austin, Texas 78713, U.S.A.

ABSTRACT

The Lower Cretaceous Pettet (Sligo) Formation of East Texas has been a target for hydrocarbon production for over 85 yr. The formation preserves a record of a long-lived carbonate platform with an extensive 125+ mi (200+ km) wide platform interior containing a complex mosaic of ooid-skeletal grainstones, argillaceous skeletal-green algal packstones, siliciclastic-rich molluscan packstones, and siliciclastic mudstones. The shoals are ubiquitous across East Texas and are the reservoir facies for dozens of fields in the region. However, they commonly interfinger with other facies at a meter scale, and well-to-well connectivity is sometimes unexpectedly poor, raising questions of lateral continuity and extent of shoal bodies. To address these problems, this study presents a comprehensive analysis of the facies, sequence stratigraphy, and stratal architecture of the Pettet Formation in Rusk County, East Texas, and identifies the geographic and stratigraphic distribution of shoal intervals within four defined subunits. Facies analysis reveals that shoal packages follow a consistent upsection progression from skeletal to ooid grainstones within each subunit. Porosity and permeability measurements demonstrate that basal skeletal grainstones have the greatest reservoir quality, while capping ooid grainstones and off-shoal facies are tight. Maps of grainstone distribution within each subunit reveal trends in shoal positioning that indicate eustatically-controlled changes in accommodation and reflect depositional diachroneity across the study area. The delineation of two third-order composite sequences, which are correlative to two of four third-order sequences (Barremian–30 and Aptian–10) described in the Sligo Formation of Central Texas, suggests that carbonate deposition in the East Texas region initiated later than in Central Texas, likely related to East Texas's proximity to a siliciclastic source. This study's insight into the timing of Pettet Formation deposition, in addition to the contribution of the region's first detailed sequence stratigraphic framework, provides a solid foundation for new work assessing future play development.

INTRODUCTION

In the Early Cretaceous, the northern Gulf of Mexico was dominated by the Comanche Platform, a long-lived steep-rimmed carbonate platform with an extensive platform interior that stretched as much as 125 mi (200 km) inland (Phelps et al., 2014). Significant structural complexity underlying this vast platform produced variable intrashelf paleobathymetry, with localized uplifts, island highs, and depressions that affected carbonate depositional systems at local and regional scales (e.g., Loucks, 1977; Bebout et al., 1981; Kerans, 2002; Hull, 2011; Phelps et al., 2014; Sitgreaves, 2015; Hattori et al., 2019). Consequently, there are significant differences in the expression of Cretaceous carbonate deposition on this platform. The Barremian-Aptian Sligo or Pettet Formation (nomenclature dependent on geographic location) platform-building interval is a prime example of the heterogeneity that can be expected in the Comanche Platform interior.

Over the past decades, numerous studies have put a significant amount of effort into characterizing the Sligo Formation at a regional scale in South and Central Texas (e.g., Bebout, 1977; Bebout et al., 1981; Kirkland et al., 1987; Fritz et al., 2000; Phelps et al., 2014). In stark contrast, very little work has been done to characterize the East Texas Pettet Formation, which is considered to be time-equivalent to the Sligo Formation. Early work by Nichols (1958) and Nichols et al. (1968) established the general stratigraphy for the Pettet and attributed changes in thickness to interfingering of siliciclastics, but did little else to correlate stratigraphic intervals within the formation. The majority of rock-calibrated data from the Pettet is sourced from work by Wiggins and Harris (1984) and Harris and Wiggins (1985) documenting shoaling sequences and associated porosities in a single core from Rusk County, and recent work by Spears (2020) documenting Pettet depositional systems in the Wright Mountain Field in Smith County. No sequence stratigraphic framework has been developed for the region, and thus cyclicity, architecture, and regional facies distribution remain poorly constrained.

Manuscript received April 13, 2021; revised manuscript received May 21, 2021; manuscript accepted June 5, 2021.

GCAGS Journal, v. 10 (2021), p. 31–46.

Despite the paucity of available literature discussing the Pettet Formation, the formation is of significant importance to the Gulf Coast oil and gas industry and has been a prolific producer for over 80 yr. Since first discovery of hydrocarbons in the Pettet in 1936 (Nichols, 1958), over 75 reservoirs have been discovered in East Texas alone, including the giant Carthage Field (Rogers, 1968). Production is most commonly established from oolitic-skeletal shoal complexes in association with paleotopographic highs (e.g., nearshore environments, uplifts, salt domes, fault blocks) (Nichols, 1958; Wiggins and Harris, 1984; Harris and Wiggins, 1985; Hackley and Karlsen, 2014). Geologic assessments indicate that significant untapped resources remain (Hackley and Karlsen, 2014), but limited understanding of the regional stratigraphy of the formation in the context of structural features emplaced pre- or post-deposition is a barrier towards further development.

This study aims to fill this gap by establishing a core-calibrated sequence stratigraphic framework, including a nearly-complete stratigraphic section and a more robust suite of facies-calibrated porosity and permeability data, for the Pettet Formation in Rusk County, East Texas. Rusk County, which is located on a paleostructural high (Cicero et al., 2010), represents a relatively tectonically stable setting that is ideal for establishing a framework based on a combination of core descriptions and wireline-log correlations, tuned to the eustatic sea-level signal. The construction of this framework represents a major improvement in recognition of changing depositional settings through time, cyclic facies stacking patterns, shoal-complex migration, and subsequent related impacts on reservoir facies distribution and continuity of this unit within Rusk County. The architectural foundation established here will also assist in building an improved stratigraphic framework throughout East Texas, which will aid in the search for by-passed and missed hydrocarbon reservoirs.

GEOLOGIC BACKGROUND

The Lower Cretaceous Pettet Formation of East Texas records the flooding of the Comanche Platform and initiation of carbonate production in the Early Cretaceous (Hauterivian-Aptian) following extensive deposition of fluvio-deltaic siliciclastics of the Travis Peak (Hosston) Formation (Fig. 1) (Bebout et al., 1977, 1981; Dutton et al., 1990). The contact between the Pettet Formation and the underlying Travis Peak Formation is lithostratigraphically defined as the transition from siliciclastic-dominated sedimentation to carbonate-dominated sedimentation (Nichols, 1958), and is therefore time-transgressive. On the San Marcos Arch of Central Texas, siliciclastics of the underlying Hosston Formation (Travis Peak equivalent) transitioned into carbonates of the Sligo Formation (Pettet equivalent) in the transgressive systems tract of the second-order Hauterivian-Barremian 136–124 sequence (Phelps et al., 2014). The Pettet Formation has long been assumed to have been deposited contemporaneously with the Sligo Formation over the same length of time, but because the contact is lithostratigraphically defined, this may not be valid; consequently, this idea is investigated as part of this study.

During the transgressive systems tract of the Hauterivian-Barremian 136–124 sequence, contemporaneous establishment of the aggradational Sligo reef margin trend rimming the passively subsiding Comanche Platform promoted extensive carbonate accretion across the platform interior spanning hundreds of kilometers (Phelps et al., 2014) (Fig. 2A). In East Texas, the Pettet Formation is largely composed of somewhat argillaceous low-energy, shallow-water, subtidal platform-interior carbonate facies interfingered with clean, high-energy oolitic and skeletal shoals and flats that comprise the main reservoir facies (Wiggins and Harris, 1984; McFarlan and Menes, 1991). In nearshore environments, the Pettet Formation also interfingers with pulses of very fine-grained quartzarenites and siliciclastic siltstones.

Carbonate deposition was abruptly truncated across the platform in the early Aptian as a result of effects of Ocean Anoxic Event 1a (OAE1a) (Phelps et al., 2015). This OAE, which is thought to have originated by massive injection of CO_2 into the

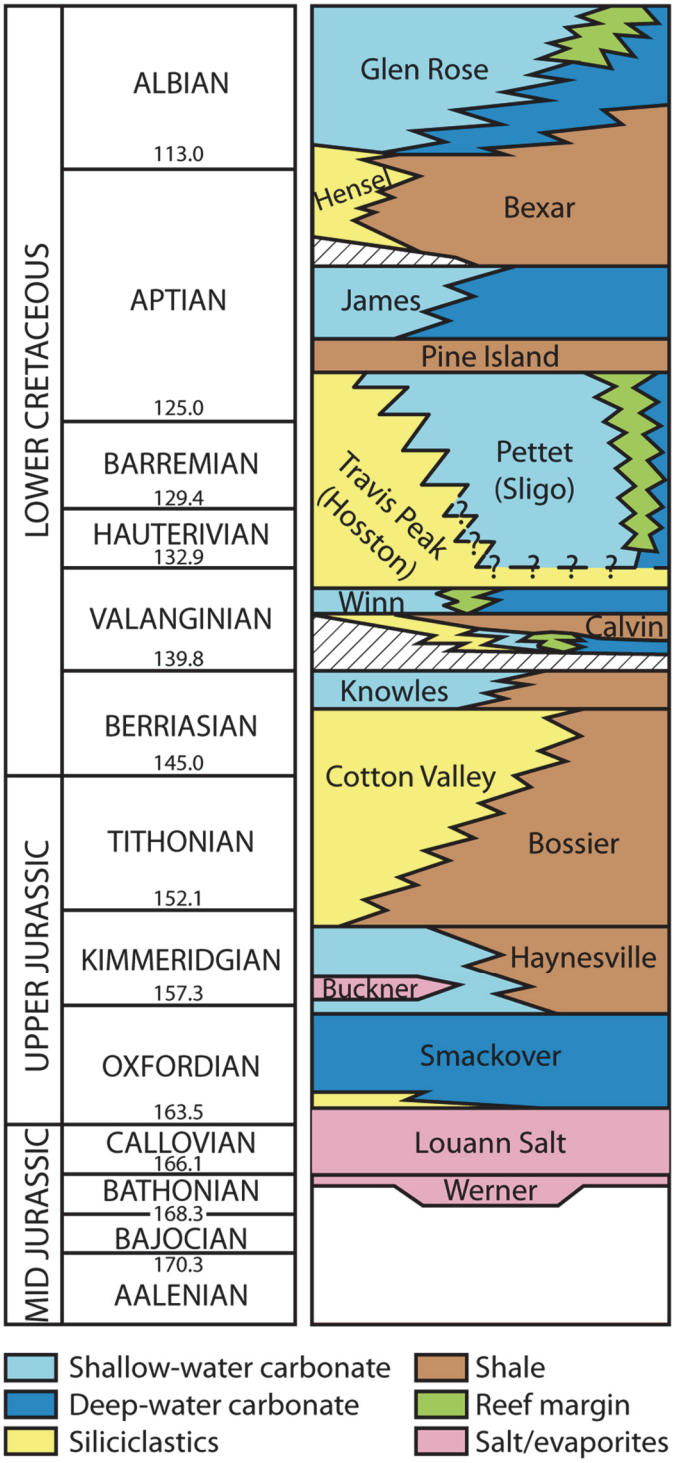

Figure 1. Stratigraphic column of the Lower Cretaceous of the northern Gulf of Mexico, including generalized lithological relationships (modified after Phelps et al. [2014] and Loucks et al. [2017], with updated age dates from Walker et al. [2018]).

atmosphere by large igneous province volcanism as well as release of methane hydrates from basinal sediments, suppressed carbonate saturation states and possibly caused surface-water acidification, effectively shutting down or greatly inhibiting the carbonate factory at a nearly global scale in a geologically instantaneous amount of time (e.g., Menegatti et al., 1998; Wissler et al., 2003; Weissert and Erba, 2004). In strata of the Comanche Platform, OAE1a manifests as a sharp transition from normal marine shallow-water carbonates of the Pettet and Sligo formations into siliciclastic mudstones of the Pine Island Shale (Loucks, 1977; Hull, 2011; Phelps et al., 2015). This contact, which represents a point in time, is a useful marker for correlation within the sequence stratigraphic framework across the platform.

To date, no detailed sequence stratigraphic framework has been developed for the Pettet Formation in East Texas, which hinders understanding of the architecture and facies mosaic on a lateral and temporal scale. However, researchers have established a robust sequence stratigraphic framework for the Sligo Formation in the San Marcos Arch region (Phelps et al., 2014), which serves as an excellent foundation for the stratigraphic framework for this study. The San Marcos Arch is a promontory that stretches over 100 mi (160 km) basinward from the Llano Uplift to the Comanche Platform shelf margin (Fig. 2A). Although the most proximal part of the arch remained topographically high throughout Sligo deposition, persistent subsidence created enough accommodation on the outer shelf to allow over 820 ft (250 m) of continuous carbonate accretion from the Hauterivian to the Aptian. Four third-order sequences were identified by Phelps et al. (2014) on the San Marcos Arch: the Hauterivian–10, the Barremian–20, the Barremian–30, and the Aptian–10. In this study, we establish correlative third-order composite sequences and compare them to those on the San Marcos Arch to draw conclusions about timing of deposition and differential influence of siliciclastics between the two regions. Importantly, the Sligo section on the San Marcos Arch also serves as a comparable reference section to assist in identifying local noneustatic environmental controls that influenced sedimentation style and rock composition in the East Texas region.

The structural setting of the Comanche Platform in East Texas is of crucial significance to the architecture of Pettet carbonates and the distribution of facies therein. Because shallow-water carbonate facies distributions are strongly impacted by water depth and energy regime, a complex paleobathymetry created a potential for equally complex facies mosaics. An isochron thickness map of the region encompassing the Upper Jurassic (upper Gilmer Limestone) through the Lower Cretaceous (Pettet Formation) published by Cicero et al. (2010) shows multiple intrashelf basins (isochron thicks) and topographic highs (isochron thins), all of which had the potential to locally modify depositional settings through their influence on water depth and current patterns (Fig. 2B). Of those features, the most topograph-

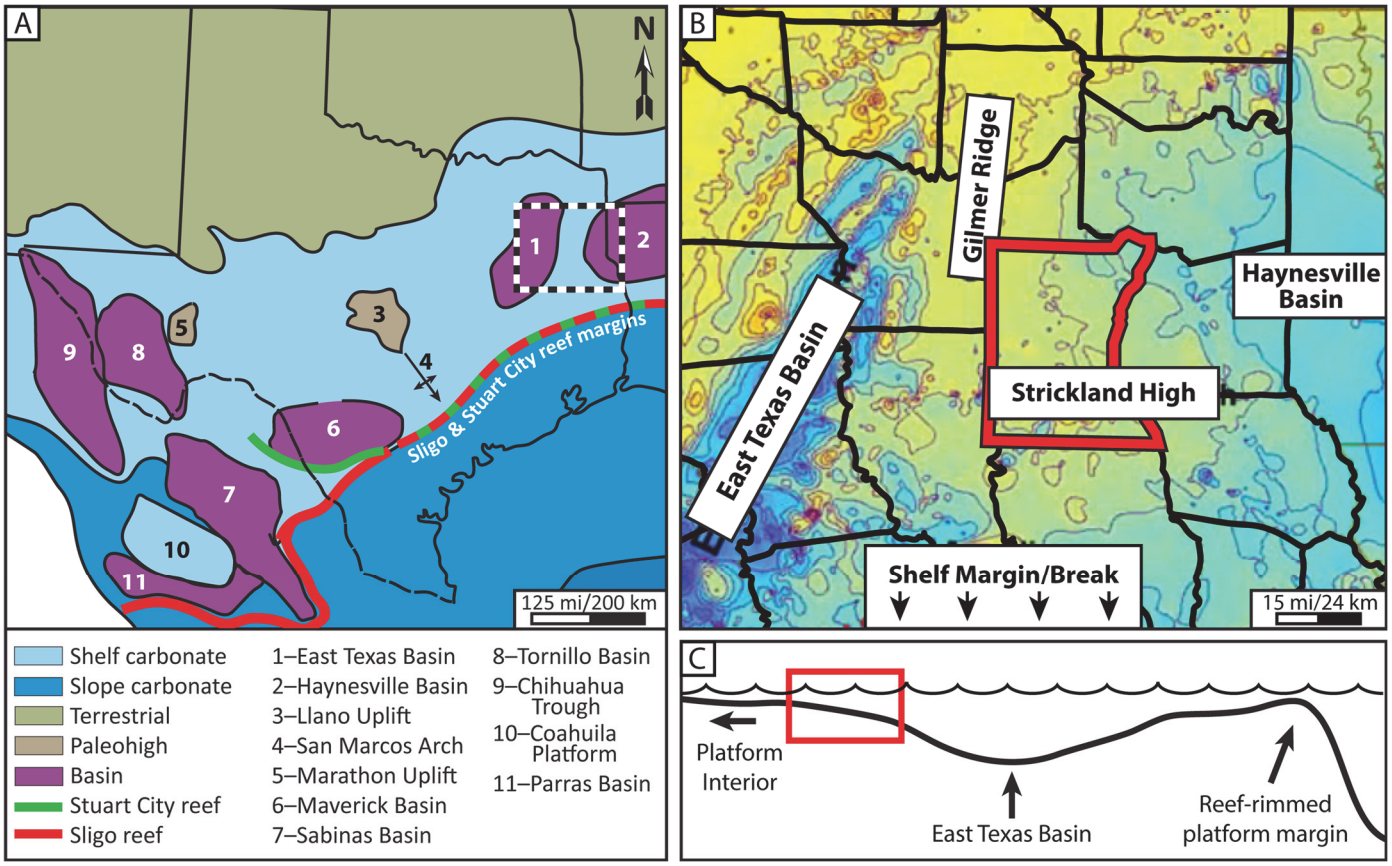

Figure 2. Regional and subregional paleogeography of the Comanche Platform in Texas and in East Texas. (A) Generalized regional paleogeographic map of Texas depicting significant structural features including basins, uplifts, and arches (modified after Phelps et al. [2014]). Box with thick dashed black and white outline indicates area shown in (B). (B) Isochron of East Texas from seismic time structure maps, depicting regional variations in thickness from the upper Jurassic Gilmer Lime through Pettet Formation interval (modified after Cicero et al. [2010]). Thicks (cool colors) represent intrashelf basins, and thins (warm colors) represent structural highs. Red outline shows study area of Rusk County, Texas. (C) Generalized dip profile of Comanche Platform depicting intrashelf features such as the East Texas Basin. Red box indicates the depositional position of the study area in the profile.

ically complex is the East Texas Basin, a salt basin that hosts dozens of salt domes and diapirs (Jackson and Seni, 1983). Another significant feature is the Haynesville Basin (Cicero et al., 2010), otherwise known as the North Louisiana Salt Basin (Lobao and Pilger, 1984). The study area, Rusk County, is located on a stable structural paleobathymetric high ("Strickland High," *sensu* Cicero et al. [2010]) just to the east of the East Texas Basin and west of the Haynesville Basin. The isochron map published by Cicero et al. (2010) portrays it as a persistent promontory dividing the two basins. Although it is located in the interior of a steep-rimmed platform, the local architecture is a shallowly-dipping ramp adjacent to an intrashelf basinal low (Fig. 2C). Its simple, gently-dipping paleobathymetry and stable structural setting is ideal for constructing a sequence stratigraphic framework calibrated to a sea-level curve, as there is little potential for other extrinsic controls (such as halokinesis) to influence facies distributions and stacking patterns.

METHODS

Wireline-log correlation was conducted using spontaneous potential (SP), resistivity, and (when available) gamma ray (GR) logs. Four Pettet subunits (A, B, C, and D) were delineated based on consistent resistivity markers that could be reliably correlated across the study area (Fig. 3). Over 1000 wireline logs were correlated in Rusk County to assist in building a robust stratigraphic framework that documents shoal facies and associated reservoir facies distribution through time (Fig. 4). Shoal complexes, which are marked by abrupt large negative SP deflections, were individually mapped within each subunit to allow analysis of shoal distribution and thickness through time. Carbonate grainstones, which comprise the majority of shoal complexes within the Pettet Formation, are devoid of siliciclastic material and thus were readily identified in the subsurface using SP and GR wireline logs. In contrast, off-shoal lower-energy platform interior facies are affected by persistent siliciclastic and clay-mineral input, which alters wireline-log response, sometimes making them appear to be similar to shales or sands. Consequently, shoals, indicated by negative SP response, were easily recognized on the wireline logs. Other subtidal facies were not as easily differentiated using standard wireline logs and instead were inferred based on their proximity to shoal complexes and their placement within cycles relative to the shoal intervals.

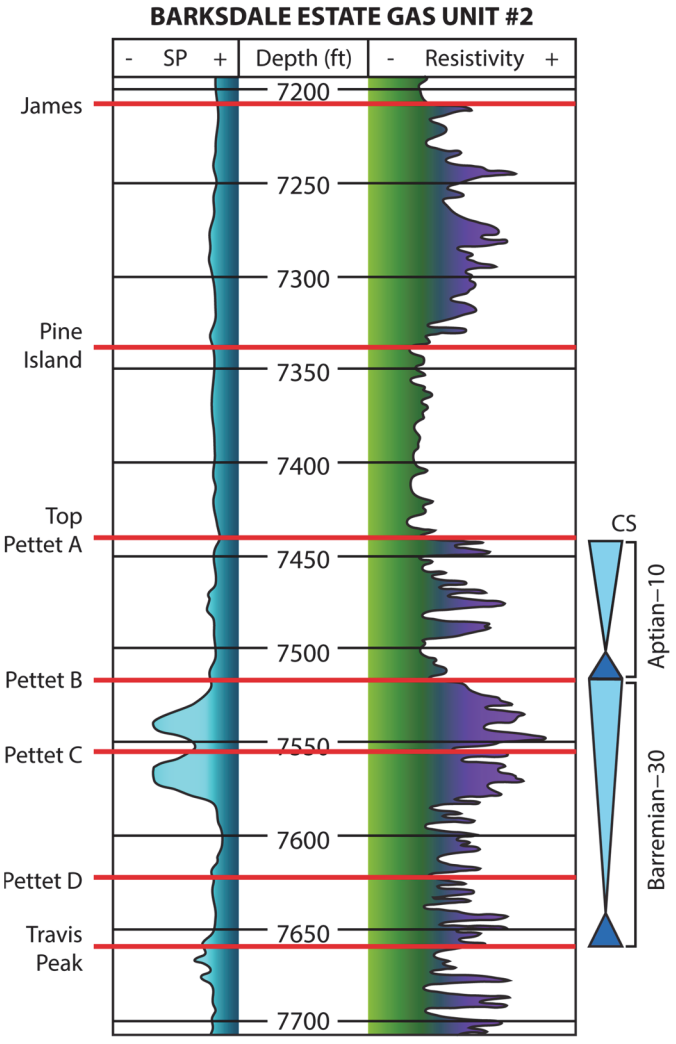

Figure 3. Example dual induction wireline log from the ARCO Barksdale Estate Gas Unit #2 well with formations and Pettet subunits labeled. Interpreted transgressive (dark blue)/regressive (light blue) composite sequences (CS) for the Pettet Formation are shown in the right-hand column.

Core descriptions and petrographic analyses were used to calibrate wireline-facies interpretations for use in subsurface correlations where no rock data is available. Seven cores, ranging in length from 46 to 120 ft (15 to 37 m), were described from the study area (Table 1). It should be noted that one core, the Kleuppel #1, is located in Smith County just to the west of Rusk County. It was necessary to include this core in this study because it is the only core that the authors had access to in this region that recovered the Pettet A subunit. Petrographic analysis was conducted on 118 standard-sized (1 in by 2 in) thin sections, impregnated with blue epoxy, to verify the grain composition of different facies and to examine pore types as well as diagenetic alteration.

Porosity and permeability analyses were conducted for 40 core plug samples taken from three cores: Kleuppel #1 (15 samples), Barksdale Estate Gas Unit #2 (13 samples), and Haskins #1 (12 samples). Core-plug-sample locations were selected mostly to represent the range of reservoir facies, with a few samples representing off-shoal nonreservoir facies for comparison. Porosity analyses were conducted with the samples under net confining stresses appropriate for their corresponding burial depths. Permeability results were corrected for the Klinkenberg effect. After analysis, three plugs were found to contain a fracture, and their data were removed from consideration. All valid porosity and permeability data were separated by facies type for evaluation of reservoir quality (Table 2).

Sequence stratigraphic analysis was conducted starting with the seven described cores, in which high-frequency (fourth/fifth order) cyclicity was established on the basis of facies stacking patterns. These higher-order elements could not be delineated on wireline as they commonly fall below wireline-log resolution. Third-order composite sequences were established following shoal trajectory (progradational/retrogradational) through the stratigraphy. These data were used to build a robust core- and wireline-log-calibrated sequence stratigraphic framework for the study area.

RESULTS

Facies Descriptions

Facies of the Pettet Formation have been organized into three separate facies associations based on interpreted depositional setting: (1) high-energy shoal complex, (2) low-energy carbonate-dominated subtidal, and (3) low-energy siliciclastic-dominated subtidal.

Facies Association 1: High-Energy Shoal Complex

1a: Ooid grainstone facies (Fig. 5A). Description: The ooid grainstones are dominated by large, well-sorted ooids up to

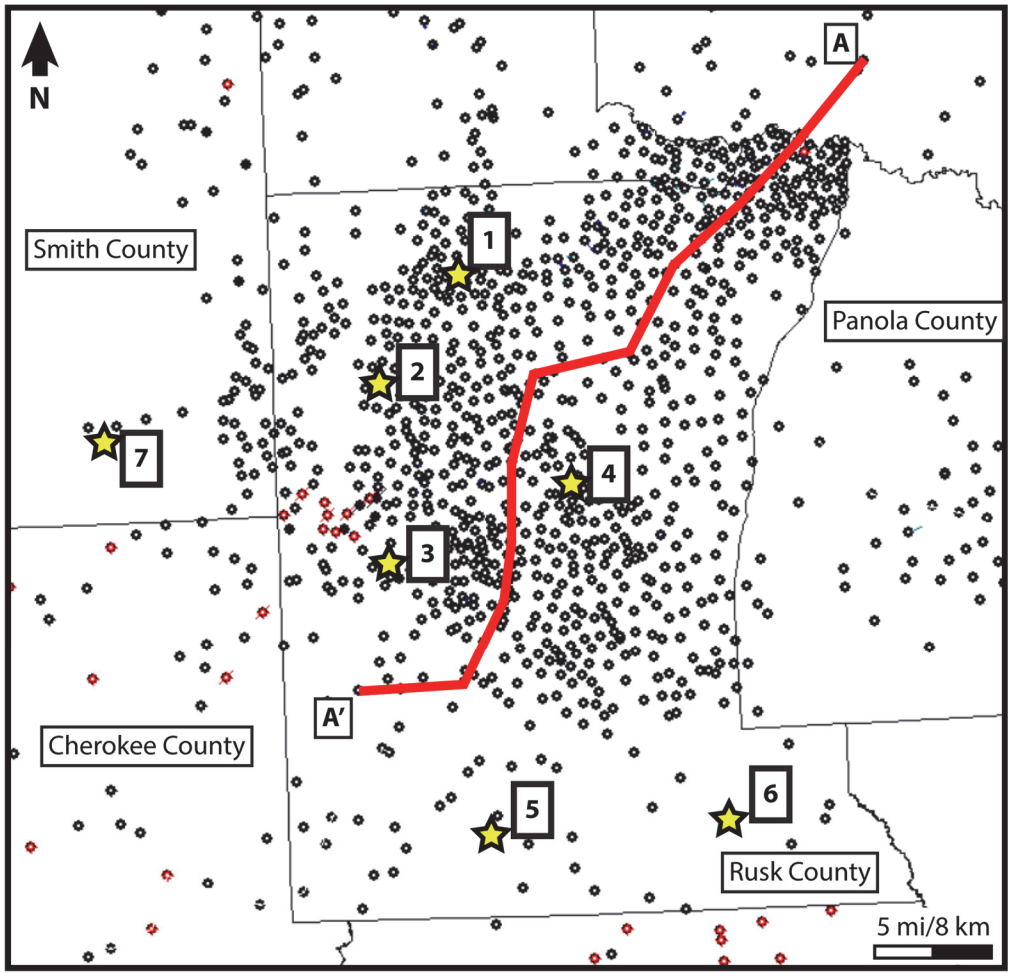

Figure 4. Map of study area showing well locations, core control, and line of cross-section. Wells used in wireline log correlation are denoted with black circles; wells with core control are labeled with numbered boxes and yellow stars. Numbers in boxes correlate to the numbered wells in Table 1. Red line traces cross-section A–A' shown in Figure 10.

Table 1. Cores shown in Figure 4, including well operator, well name, Pettet/Travis Peak intervals recovered, and length of core.

#	Operator	Lease	Formations (cored length)
1	Henderson Clay Products	Fred Beck G.U. #2	Pettet B–C (60 ft), Travis Peak (60 ft)
2	ARCO	Barksdale Est. G.U. #2	Pettet B–C (60 ft), Travis Peak (58 ft)
3	ARCO	Haskins #1	Pettet B–C (57 ft), Travis Peak (58 ft)
4	Henderson Clay Products	Jennings F.L. #1	Pettet D (36 ft), Travis Peak (41 ft)
5	Shield Resources	Alton Strickland #1	Pettet B (46 ft)
6	McCormick Oil & Gas	Frank Poulsen #1	Pettet D–Travis Peak (59 ft)
7	Map Production	Kleuppel #1	Pettet A–C (120 ft)

1.5 mm in diameter. Ooids are radial and appear to preserve original calcitic fabrics, which are commonly partially micritized. Nuclei are generally composed of peloids, echinoid plates, or molluscan fragments; miliolids may occur uncommonly as nuclei. Ooids are rimmed by a thin isopachous bladed calcite cement, sometimes with an additional outer rim of equant calcite cement, and interparticle pore space is almost always completely filled by late-stage blocky calcite. Faint low-angle planar bedding may be observed, but is uncommon. This facies is generally observed at the top of shoaling-up sequences below a transition to more mud-dominated facies.

Pore preservation is poor, with remaining porosity averaging 1.8%, and permeability averages 0.001 md (geometric mean) (Table 2). Because nearly all interparticle pore spaces have been occluded by late-stage equant calcite spar, the dominant pore type remaining is micropores, which are common in the ooids, especially those ooids that are more heavily micritized.

Interpretation: The ooid grainstone facies is interpreted to have been deposited in a high-energy shoal-complex environment and is considered to be the highest-energy facies deposited in the Pettet Formation. Although well-developed planar bedding or cross stratification is not commonly observed, the absence of carbonate mud and abundance of well-developed ooids indicates deposition in very shallow water with high flow velocities associated with strong current and wave energy, likely in a shoal-crest-type environment (Fig. 6) (e.g., Reeder and Rankey, 2008; Harris et al., 2015, 2019). Two episodes of early cementation are recorded, with the first isopachous bladed calcite cements rimming grains being indicative of a marine-phreatic early diagenetic environment, and equant calcite overgrowths deposit-

Table 2. Statistical data for results of porosity and permeability analyses conducted on 37 core plug samples representing four facies. Note that for samples that were below permeability detection limit (<0.0001 md), a value of 0.0001 md was used for statistical analyses.

Facies		Porosity					Permeability					
		Mean (%)	Std. Dev. (%)	Min. (%)	Max (%)	Count	Mean (md)	Geom. Mean (md)	Std. Dev. (md)	Min. (md)	Max. (md)	Count
1a	Ooid grainstone	1.8	1.2	0.1	3.3	7	0.007	0.001	0.016	<0.0001	0.043	7
1b	Superficial oolitic-skeletal grainstone	4.9	3.2	0.2	9.9	16	0.289	0.011	0.741	<0.0001	2.990	16
1c	Skeletal grainstone	9.4	5.9	1.3	18	10	12.222	0.145	20.147	0.0004	51.990	10
2a	Off-shoal skeletal packstone	0.05	0.6	0.2	1.4	4	0.001	0.0004	0.001	0.0001	0.002	4

ed later in a meteoric-phreatic regime (Halley and Harris, 1979; Harris, 1979; Longman, 1980). The presence of both types of cements suggests that early cementation occurred in a very shallow-water environment with abundant water flow, and then was influenced by a later influx of meteoric water during subaerial exposure.

1b: Superficial oolitic-skeletal grainstone facies (Fig. 5B). Description: The superficial oolitic-skeletal grainstone facies is characterized by a mixture of radial calcitic ooids, uncoated skeletal grains, and skeletal grains possessing a thin superficial oolitic coating. Skeletal grain types include abundant subrounded to rounded calcareous green algae (mainly dasyclads and udoteaceans), echinoid, and molluscan fragments, as well as peloids and miliolids. The ratio of true ooids to superficial ooids to uncoated skeletal grains is variable, with greater dominance by true ooids towards the tops of individual beds and cycles, and greater dominance by uncoated skeletal grains towards the base of cycles. Cementation dominantly consists of equant calcite cements rimming grains, with some larger equant calcite spar occluding interparticle pore space.

Reservoir quality of this facies is poor to fair, with porosity averaging 4.9% and permeability averaging 0.011 md (geometric mean) (Table 2). The dominant pore type is interparticle, with some dissolved grains (most commonly ooids and calcareous green algae fragments, respectively) contributing to moldic pores. Micropores are also common in micritized grains.

Interpretation: The superficial oolitic-skeletal grainstone facies was deposited in a moderate- to high-energy sand-flat environment, similar to that of the ooid grainstone. However, its greater abundance of skeletal grains and lower abundance of well-developed ooids indicates that this facies was likely deposited in slightly lower-energy conditions than that of the ooid grainstone. Superficial ooids are commonly attributed to a slightly lower-energy environment in which grains are tumbled less before final deposition, resulting in a thinner oolitic coating (e.g., Carozzi, 1957; Strasser, 1986; Flügel, 2010). Equant calcite cements rimming grains are most likely meteoric-phreatic in origin (Longman, 1980).

1c: Skeletal grainstone facies (Fig. 5C). Description: The skeletal grainstone facies is composed almost entirely of skeletal grains possessing no superficial oolitic coating. Skeletal grainstone composition is variable but most commonly consists of calcareous green algae (dasyclad and udoteacean) fragments, as well as echinoid plates, mollusk fragments, miliolids, and peloids. Ooids and superficial ooids are rare or absent. Grains are moderately rounded, and are commonly rimmed by equant calcite cements; later-stage larger equant calcite spar is uncommon but may occlude some interparticle pores.

(FACING PAGE) Figure 5. Facies of the Pettet Formation. (A–C) High-energy shoal complex facies association. (A) Ooid grainstone, photomicrograph in plane polarized light (PPL). Note preserved radial texture in ooids that indicates that they were originally calcitic. (B) Superficial oolitic-skeletal grainstone, photomicrograph in PPL. Most grains have a superficial oolitic coating that is not well-developed enough to constitute a true ooid. (C) Skeletal grainstone, photomicrograph in PPL. Skeletal grains are largely uncoated, and significant interparticle pore space is retained. (D–H) Low-energy carbonate-dominated subtidal facies association. (D) Argillaceous miliolid-skeletal-green algae packstone, core photograph. Note common allochthonous ooids and superficial ooids mixed in with oysters, lime mud, and argillaceous wisps in this interval. (E) Argillaceous miliolid-skeletal-green algae packstone, photomicrograph in PPL. Dasyclads, miliolids, and peloids are abundant; some broken ooids and abraded intraclasts are present. (F) Chondrodont-toucasid floatstone, core photograph. Chondrodonts are undamaged and likely preserved in situ. (G) Siliciclastic-rich molluscan packstone, photomicrograph in PPL. The fauna are limited to mollusks with no miliolids or calcareous green algae present; note decreased skeletal grain abundance and increased percentage of quartz silt as well. (H) Rippled lenticular-bedded siliciclastic mudstone, core photograph. Dark-colored part of core is faintly laminated siliciclastic mudstone; light-colored rippled part is composed of slightly coarser quartz silt.

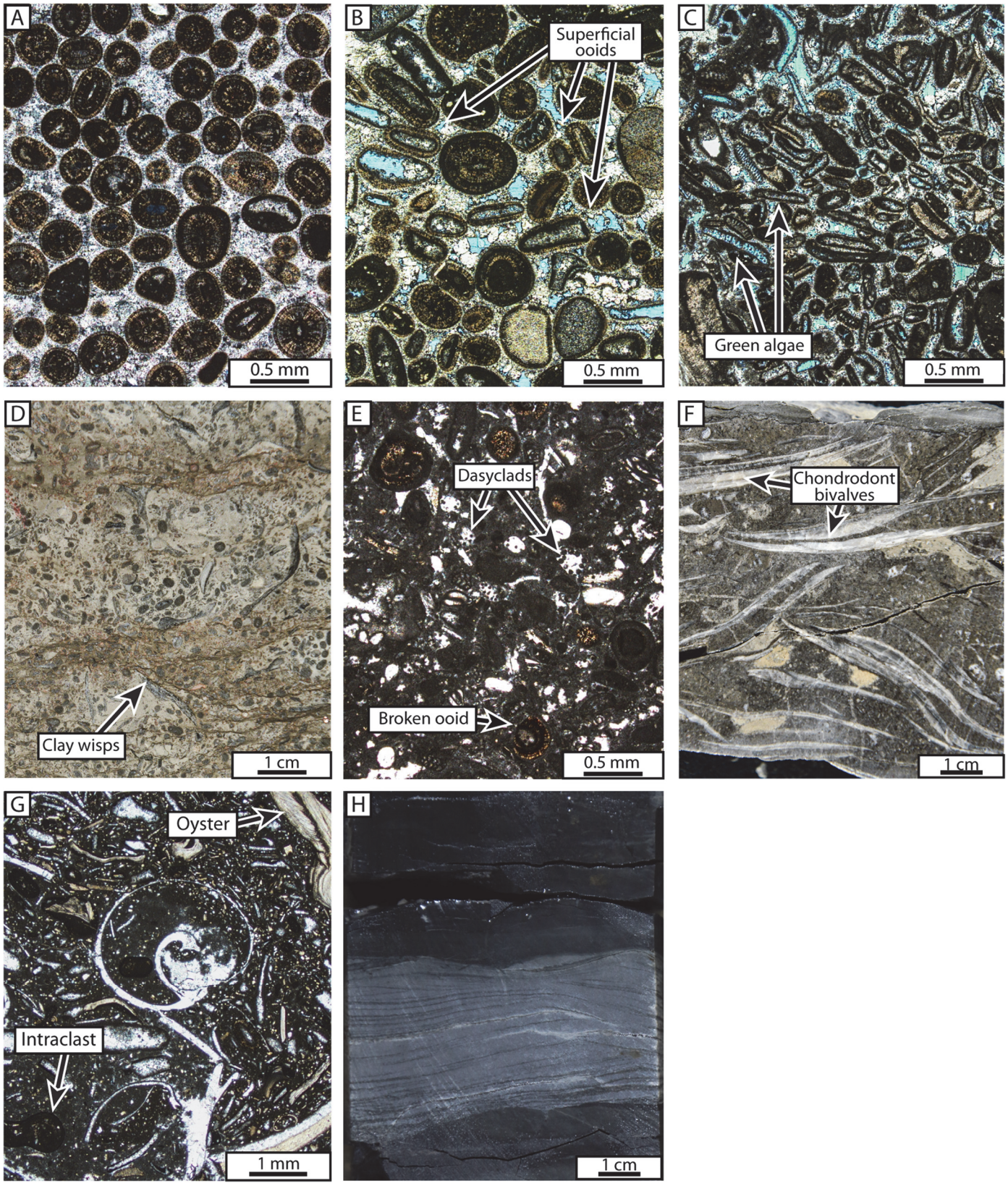

The skeletal grainstone facies represents the best reservoir facies, with porosity averaging 9.4% and permeability averaging 0.145 md (geometric mean) (Table 2). The maximum porosity recorded was 18%, and the maximum permeability recorded was 51.99 md. Porosity is high because of the excellent retention of interparticle pore space as well as significant contribution from dissolved grains; calcareous green algae and molluscan fragments (originally aragonite) were particularly susceptible to dissolution in this facies, leaving behind large moldic pores that remained unfilled.

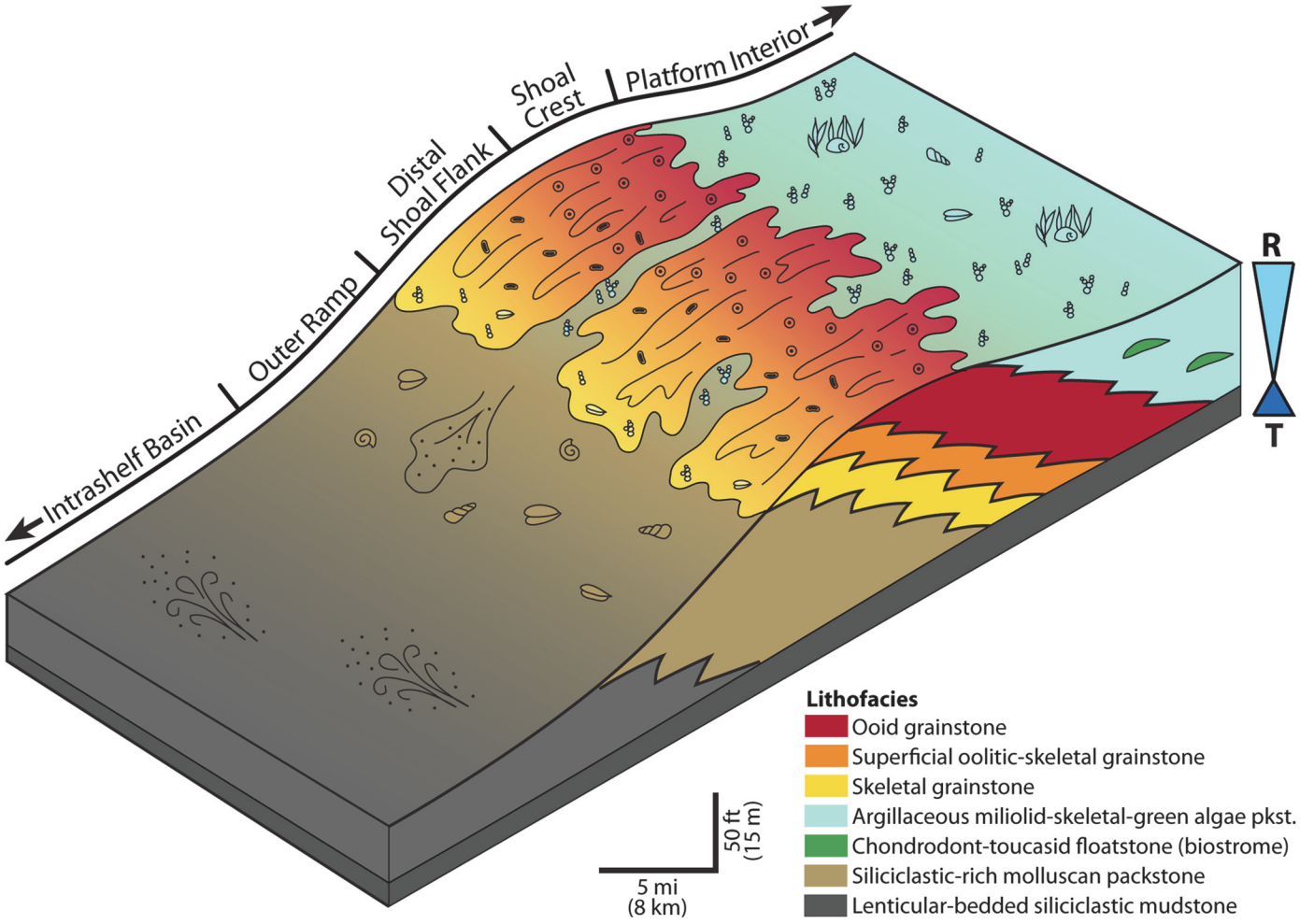

Figure 6. Depositional model for the Rusk County intrashelf ramp depicting environments represented in this study during a transgressive-regressive sequence. Note that model is not drawn to scale, and has been vertically exaggerated.

Interpretation: The high degree of grain reworking as well as the absence of mud filling interparticle pores in the skeletal grainstone facies is indicative of a high-energy sand-flat environment within a shoal complex. Grains did not acquire superficial oolitic coatings, which could be attributed to a lower amount of time in the swash zone prior to final deposition, or absence of conditions needed to develop oolitic coatings (e.g., higher energy current and wave action, seawater adequately supersaturated in carbonate, or microbial mediation of precipitation; see Harris et al., 2019).

Facies Association 2: Low-Energy Carbonate-Dominated Subtidal

2a: Argillaceous miliolid-skeletal-green algae packstone facies (Figs. 5D and 5E). Description: The argillaceous miliolid-skeletal-green algae packstone facies is characterized by a diverse assemblage of carbonate grains in a lime mud matrix, very commonly argillaceous with clay seams readily visible in core. The most abundant grains are fragments of calcareous green algae (dasyclad and udoteacean), mollusks (formerly aragonitic bivalves, chondrodonts, toucasid rudists, and oysters), and echinoids. Miliolids are also abundant. Ooids, superficial ooids, grapestones, gastropods, and other benthic foraminifers may be present. Grains are poorly sorted and exhibit a broad range of angularity from angular to rounded. Whereas most skeletal grains are commonly angular to subangular and display few signs of reworking, ooids, superficial ooids, and grapestones are commonly abraded and heavily micritized.

The argillaceous miliolid-skeletal-green algae packstone facies is a poor reservoir facies. Porosity averages 0.05% with a maximum recorded value of 1.4%, and permeability averages 0.0004 md (geometric mean) with a maximum recorded value of 0.002 md. The dominant pore type is micropores with lesser moldic pores. Interparticle pores were not observed.

Interpretation: Abundant lime mud and a diverse shallow-water biota suggest that the argillaceous miliolid-skeletal-green algae packstone was deposited in a low-energy, shallow-water environment, likely in a local inner ramp setting landward of the shoals (Fig. 6). Skeletal grains appear to be autochthonous as they exhibit very little mechanical abrasion. In contrast, the abrasion of ooids, superficial ooids, and grapestones suggests an allochthonous origin, likely derived from washover from a nearby shoal complex.

2b: Chondrodont-toucasid floatstone facies (Fig. 5F). Description: The chondrodont-toucasid floatstone facies is a carbonate-dominated facies that is readily recognized by the presence of clusters of large, whole chondrodont clams or toucasid rudists (or both). These macrofauna are commonly preserved in life position (upright orientation for chondrodonts, or reclining for toucasids) floating in a skeletal-peloidal wackestone to packstone matrix. Associated skeletal grains include abundant miliolids and common calcareous green algae, echinoid, and molluscan

fragments; these are poorly sorted and range from angular to subrounded. Ooids and superficial ooids are rarely observed, and may be broken.

Interpretation: Well-preserved chondrodonts and toucasids, intact and in life position, are indicative of growth in a low-energy, shallow-water subtidal environment (Perkins, 1974; Scott, 1981; Hofling and Scott, 2002; Kerans, 2002). Because these macrofauna are commonly clustered together, it is likely that this facies represents a biostrome setting (Fig. 6). These biostromes are reported to reach 30 to 300 m (100 to 1000 ft) in diameter in outcrop examples (Kerans, 2002), suggesting that they cannot be correlated between much more widely spaced wells.

2c: Siliciclastic-rich molluscan packstone facies (Fig. 5G). Description: The siliciclastic-rich molluscan packstone is a mixed carbonate-siliciclastic facies that contains carbonate skeletal grains and lime mud, as well as a significant amount of quartz silt and terrigenous clay minerals (~15–40% composition). The fossil assemblage is dominated by a molluscan fauna including oysters, formerly aragonitic bivalves, and small gastropods; echinoids are also common. These grains are commonly angular with little evidence of reworking. Calcareous green algal fragments and superficial ooids may be present, but are generally rare and appear abraded when present. Subrounded intraclasts consisting of similar carbonate packstone material are common.

Interpretation: The abundant lime mud observed in this facies suggests a low-energy setting, as does the low degree of mechanical abrasion of molluscan grains. The near absence of miliolids, calcareous green algae, and other shallow-water fauna indicates that this facies was deposited in a deeper subtidal setting, likely seaward of the shoal complexes (Fig. 6). Superficial ooids and calcareous green algae fragments were likely sourced from updip and became increasingly abraded or broken as they were transported into the middle-outer ramp environment or reworked significantly by intense bioturbation.

Facies Association 3: Low-Energy Siliciclastic-Dominated Subtidal

3a: Lenticular-bedded siliciclastic mudstone facies (Fig. 5H). Description: The lenticular-bedded siliciclastic mudstone facies is the only siliciclastic-dominated facies observed in the Pettet succession within the study area. Generally dark brown to black and composed largely of siliciclastic clay and silt, it commonly features light-colored rippled lenticular beds composed of coarser quartz silt but is otherwise relatively homogeneous, appearing rippled or weakly laminated to massively bedded. It reacts very weakly when treated with hydrochloric acid, and thus likely contains a very low percentage of lime mud. Oyster and other bivalve fragments are rarely observed, most commonly occurring in small cm-scale graded event beds. Pyritization is common, especially along bedding planes.

Interpretation: The lenticular-bedded siliciclastic mudstone represents a low-energy, deeper subtidal environment below fair-weather wave base. Rippled lenticular beds reflect subtle bottom-current activity (Shanmugam et al., 1993; Shanmugam, 2000). This facies is only observed in major transgressive packages in which the shelf was substantially flooded and the main carbonate factory was either shut down or transitioned updip; therefore, an open-marine, deeper water environment is the most likely depositional setting (Fig. 6).

Porosity and Permeability Analyses

Porosity and permeability analyses were conducted for 37 core plug samples representing four of the most common Pettet facies (ooid grainstone, superficial oolitic-skeletal grainstone, skeletal grainstone, and argillaceous miliolid-skeletal-green algae packstone); analytical results for each sample are reported relative to facies on a scattergram (Fig. 7). Table 2 reports the relevant statistical data for these tests, again parsed out by facies. Sampling focus was concentrated on shoal and shoal-proximal facies, as those have traditionally been the targets for petroleum exploration and production; less-frequently encountered facies (e.g., chondrodont-toucasid floatstone, lenticular-bedded siliciclastic mudstone) were not sampled.

The skeletal grainstone facies had the highest overall porosity values, with a mean of 9.4% (n = 10). Off-shoal argillaceous miliolid-skeletal-green algae packstones had the poorest porosity with a mean of 0.9% (n = 4). The lowest recorded porosity was 0.1%, in a well-cemented ooid grainstone sample; the highest recorded porosity was 18.0%, in an interparticle-pore-rich skeletal grainstone sample.

The skeletal grainstone facies also exhibited the highest overall permeability values, with a geometric mean of 0.145 md

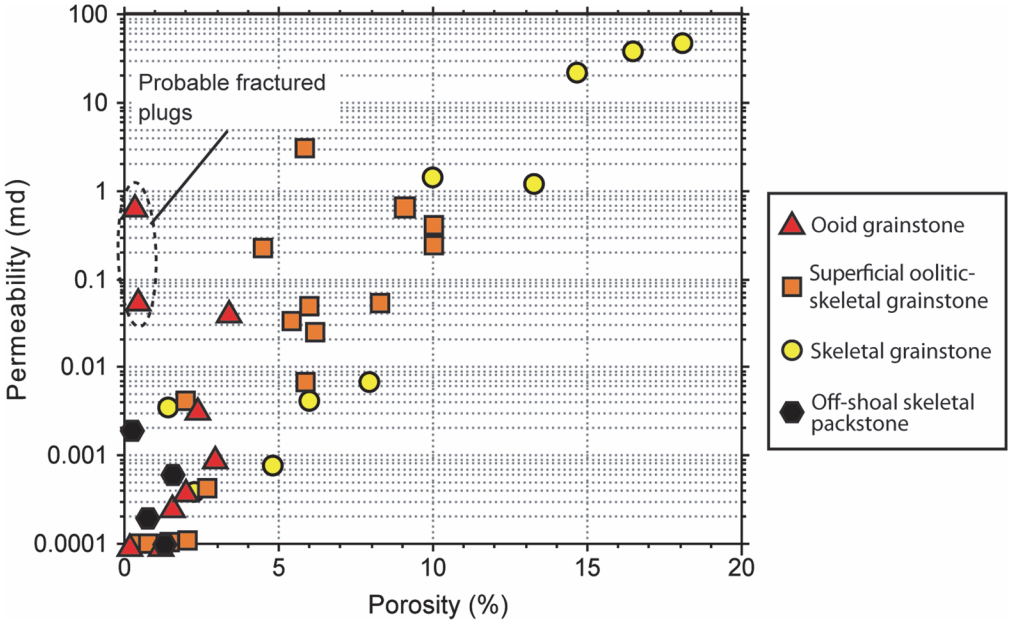

Figure 7. Scattergram of porosity versus permeability values separated by facies for samples obtained from core plug analysis of the four most common facies. Note that for analyses in which permeability values were below detection limit (<0.0001 md), a lower-limit value of 0.0001 md was assigned.

(n = 10). Once again, the off-shoal skeletal packstone facies had the lowest average permeability with a geometric mean of 0.0004 md (n = 4). The lowest recorded permeability measurement was 0.0001 md, which is the lower detection limit for these analyses, meaning that permeability could have potentially been even lower. This value was recorded in the off-shoal skeletal packstone, the ooid grainstone, and the superficial oolitic-skeletal grainstone; only the skeletal grainstone had all samples above detection limit. The highest recorded permeability was 51.99 md, which was recorded in a skeletal grainstone sample.

Cyclicity and Sequence Stratigraphy

Pettet carbonate shoaling cycles in Rusk County follow a predictable and uniform stacking pattern in the A, B, and C subunits (e.g., Figures 8 and 9); the D subunit mostly differs in the inclusion of substantially more quartz silt and less well-developed shoal complexes. High-frequency sequence (HFS) bases are commonly siliciclastic-dominated mudstones or highly argillaceous or quartz-rich lime packstones to lime wackestones representing the deepest-water transgressive facies of the succession. Shallowing upwards in the regressive portion of the cycle is reflected by a transition into low-energy subtidal siliciclastic-rich molluscan packstones. High-energy skeletal grainstones overlie those, and transition up section into superficial-oolitic skeletal grainstones. Ooid grainstones form the top of the shoal portion of the cycle. Up section from there, facies either proceed back into siliciclastic-rich molluscan facies, or transition into miliolid-green algae-skeletal-peloid wackestones and packstones with scattered biostromes distributed throughout. This succession is observed in each core of the Pettet A, B, and C units described in the study area, rarely with any deviation in stacking pattern (Figs. 8 and 9). One exception is the lower Pettet A, which exhibits siliciclastic mudstones interfingered with argillaceous miliolid-skeletal-green algae wackestones and packstones in the Kleuppel #1 core (Fig. 9)

A dip-oriented (northeast to southwest) cross-section with shoal intervals (negative SP peak) highlighted clearly demonstrates different shoal loci and shoal complex extent within each subunit (Fig. 10). Individual shoal complexes in the Pettet A, B, and C subunits are revealed to have a strongly progradational trajectory; in wells where multiple shoals stack, they are commonly separated by thin intervals of argillaceous lime packstones or wackestones (e.g., Figures 8 and 9). The Pettet B and C subunits are shown to have the most extensive shoal complexes in the study area (Figs. 10 and 11), and it is common for B and C shoals to stack across a large portion of Rusk County.

Based on overall shoal trajectory within the Pettet Formation, two complete third-order composite sequences (CS) can be delineated (Fig. 10). Transgression in the lower CS began with flooding of the shelf in the lower Pettet D. In the regressive portion of the lower CS, starting in the upper Pettet D, multiple shoal complexes developed through time and prograded downdip to the southwest, reaching maximum seaward extent at the end of Pettet B deposition (Figs. 11B–11D). The following transgression, which is associated with a significant backstepping of shoals 50 km to the northeast in the lower Pettet A, defines the transgression of the upper CS (Fig. 11E). The following regressive period in the upper Pettet A is associated with shoal complexes prograding to the southwest once more (Fig. 11F). Maximum regression of the upper CS concluded at the top of the Pettet A; deposition of the overlying Pine Island Shale followed thereafter.

DISCUSSION

Depositional Environments

Net thickness maps (Fig. 11) and general shoal-complex trajectories in the Pettet Formation demonstrate that, at time of

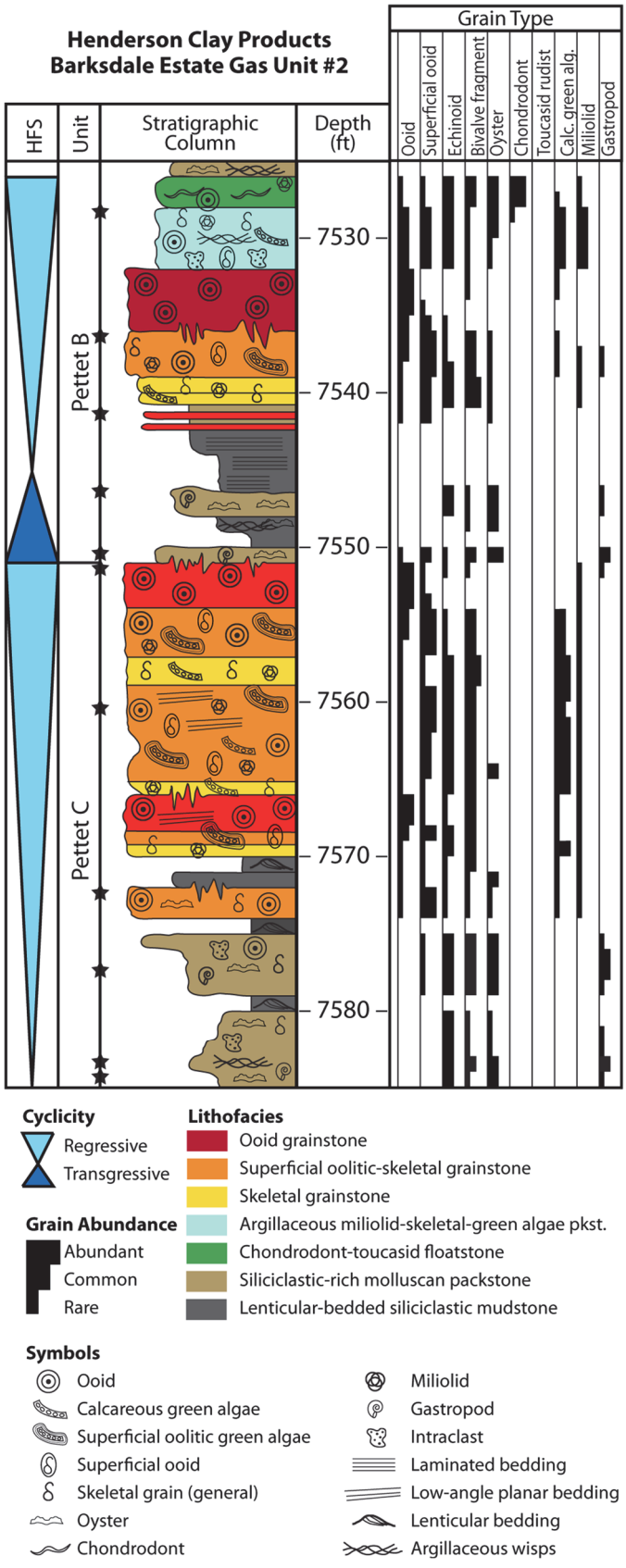

Figure 8. Core description for the Henderson Clay Products Barksdale Estate Gas Unit #2 well. Core recovers a continuous section of the Pettet B and C subunits. Note exceptionally consistent facies stacking patterns.

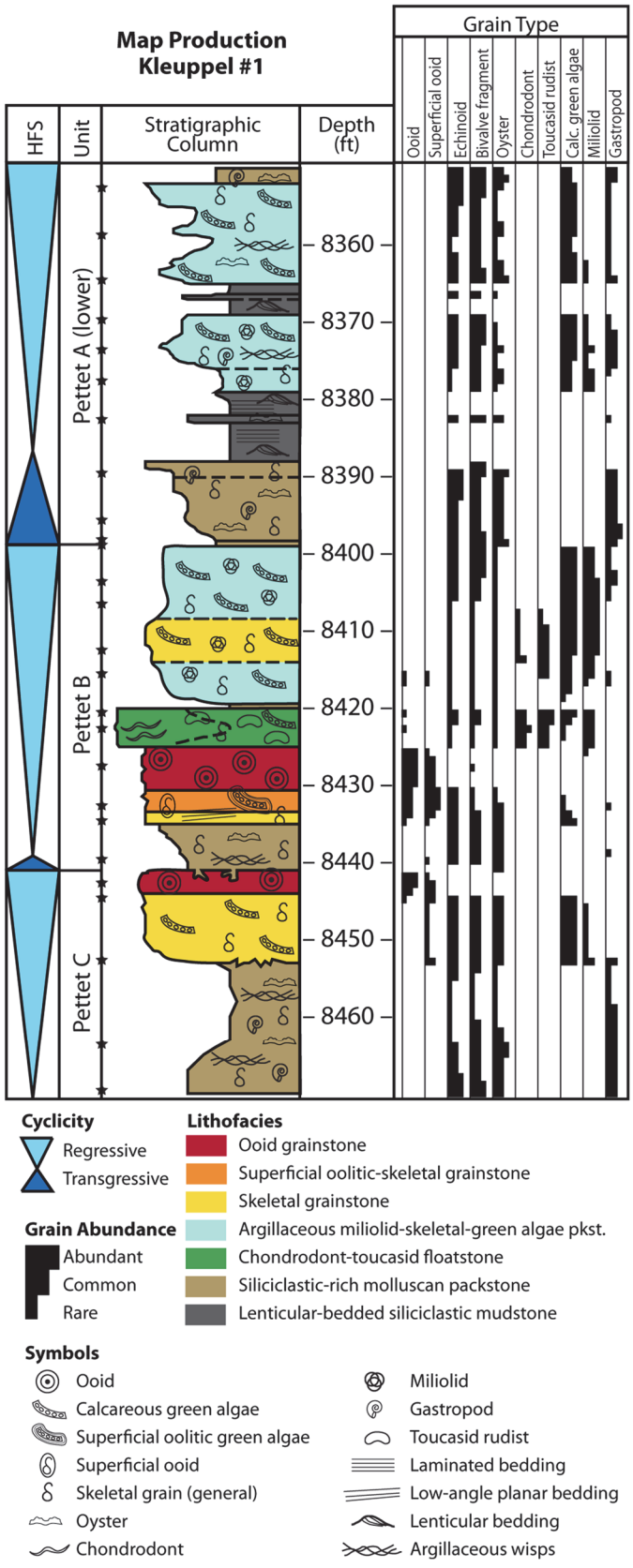

Figure 9. Core description for the Map Production Co. Kleuppel #1 well. Core recovers a continuous section of the lower Pettet A through the base of the Pettet C. Note that the Pettet C shoal interval is much thinner in this core than in other cores described in Rusk County, likely because it was located at the most distal margin of the Pettet C shoal complexes. Consistent facies stacking patterns break down somewhat following transgression at the onset of Pettet A deposition; this may be related to reorganization of facies partitioning on the shelf caused by filling of nearly all available accommodation during Pettet B deposition.

deposition, Rusk County was a part of a stable paleobathymetric high that dipped gently to the southwest towards the East Texas Basin as a very low-angle intrashelf ramp within the broader Comanche platform interior. Most shoal complexes in the county developed on this structure, although some irregular shoals also developed on fault blocks in the extreme southern end of the study area in the Mount Enterprise Fault Zone (e.g., Figures 11C and 11D). Facies stacking patterns and occurrences are consistent in all cores in all subunits across the study area (e.g., Figures 8 and 9), indicating that there was no major alteration in depositional environments throughout Pettet deposition. Local shelf architecture appears to have remained relatively consistent, with shoal complexes forming a migratory subtle intrashelf ramp crest that prograded across the area over time as a result of accommodation limitation. The increases in total formation thickness to the south-southeast (Fig. 11A) are not purely linked to shoal-complex development, but may instead represent the influence of increased subsidence rates in the Haynesville Basin (Cicero et al., 2010) and changing accommodation related to syndepositional faulting in the Mount Enterprise Fault Zone (Jackson and Wilson, 1982).

HFS facies stacking patterns provide insight into depositional environments that were present in the study area during Pettet deposition, and highlight how facies are partitioned across a dip profile (Fig. 6). During periods of no shoal development, the intrashelf ramp was dominated by siliciclastic mud deposited in a low-energy subtidal regime influenced by bottom currents, which produced the siliciclastic mudstones and rippled lenticular beds observed in core. Carbonate facies dominated the updip intrashelf ramp environments. In the middle-outer intrashelf ramp, siliciclastic-rich molluscan packstones were deposited in a low-energy, moderately deep subtidal regime. In shallower, moderate-energy environments, calcareous green algae (predominantly dasyclad and udoteacean) meadows proliferated. Although some grains from these green algae meadows are preserved relatively intact in carbonate mud matrix in core, most green algae were broken down and incorporated into the margins of the shoal complexes as the main skeletal grain type. The moderate- to high-energy environment of the distal portion of the shoal complex provided ample wave energy to rework green algae fragments, along with other molluscan and echinoid skeletal fragments, winnowing out mud and resulting in the deposition of skeletal grainstones. Closer to the shoal crest, these skeletal grains were turned into superficial ooids as thin layers of calcium carbonate precipitated around them. At the shallowest part of the shoal complexes, in the highest energy regime, an ooid factory produced a proliferation of calcitic ooids that became the dominant grain in the ooid grainstones found at the tops of shoaling intervals. These grainstones, ranging from massive to low-angle planar bedded, lack any sedimentary evidence for an attachment to shoreline (e.g., birdseye fenestrae, tidal flats, root zones, etc.), and thus are interpreted to have been deposited in a shoal complex that developed on a mid-ramp crest on the intrashelf ramp. Landward of the shoal complexes, argillaceous miliolid-green algae-skeletal-peloid packstones made up the majority of sediments deposited in the lower-energy shallow-water setting of the inner intrashelf ramp. Chondrodonts, toucasid rudists, and oysters colonized the muddy seafloor, creating biostromes of unknown extent that baffled skeletal sediments as well as mud.

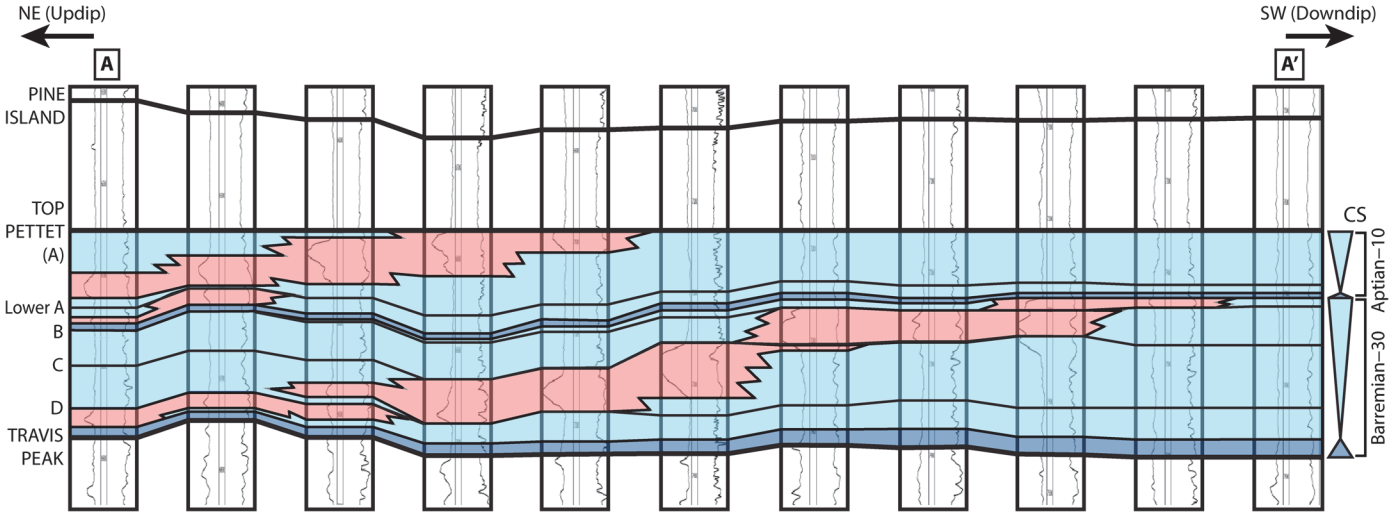

Figure 10. Dip-oriented cross-section A–A'. Two composite sequences (CS) are shown, with regressive portions colored light blue, and transgressive portions colored dark blue. Shoals are highlighted in pink to demonstrate their distribution within the Pettet subunits as well as their strongly progradational characteristics during highstand. Line of cross-section is shown in Figure 4.

The consistent facies stacking patterns observed in the Pettet B and C subunits were temporarily disrupted in the lower Pettet A during and just following the transgression of the upper CS. In the lower Pettet A, lenticular-bedded siliciclastic mudstones commonly associated with outer ramp environments were observed interfingering with argillaceous miliolid-skeletal-green algae packstones and wackestones, which are more common to inner ramp environments (Fig. 9). The disruption in facies stacking pattern could be explained as a reorganization of facies distributions across a dip profile at a time of transgression just after peak highstand (during which time nearly all accommodation in the study area had been filled and the shelf was at its flattest). At this time, small-scale eustatic fluctuations could cause unusual facies stacking patterns. The change in facies stacking patterns and associations ultimately proved to be short-lived, as shoal complexes became reestablished in northeastern Rusk County at the end of lower Pettet A deposition (Fig. 11E), and shoal complex progradation resumed in the upper Pettet A (Figs. 10 and 11F).

Timing of Shoal Development

This study's establishment of the first stratigraphic framework for the Pettet Formation in Rusk County provides context for the timing of shoal complex deposition throughout two CS. Numerous shoal complexes developed and prograded during Pettet deposition, forming distinct bodies rather than occurring as a blanket across the entire study area (Fig. 11). The Pettet A and D shoal complexes were limited to the northeastern portion of Rusk County, with the exception of the lowermost Pettet A shoals, which occurred in the southwestern portion of the county (Figs. 11B, 11E, and 11F). In contrast, the Pettet B and C shoal complexes were much larger, spreading across the majority of northern and central Rusk County (Figs. 11C and 11D). Shoals were flanked both up- and down-dip by argillaceous mud-rich facies (argillaceous miliolid-skeletal-green algae packstones, chondrodont-toucasid floatstones, and siliciclastic-rich molluscan packstones); these were deposited overlying shoaling intervals during transgression or prolonged highstand periods in which shoals migrated seaward because of limited available accommodation. These low-porosity, low-permeability facies later became stratigraphic seals. Thus, each shoal complex is likely to occur as a segregated body with poor connectivity with other Pettet shoal complexes that may be stacked in the stratigraphy (e.g., Figs. 8 and 9).

These findings have important implications for field development and production strategies. Wells may penetrate one or more shoal complex; if multiple shoals are penetrated, connectivity between them is likely to be poor as a result of low-porosity, low-permeability argillaceous mud-rich facies separating them and acting as a vertical flow barrier. Well-to-well connectivity may also be a problem if wells penetrate different shoal bodies entirely. With this new architectural framework and an improved understanding of shoal distribution in the region, we will be able to better anticipate these problems, improving field development efforts as well as enabling better-informed assessment of new prospects.

Reservoir Facies Properties

Porosity and permeability analyses demonstrate that facies type has a significant impact on reservoir quality in the Pettet Formation (Table 2 and Figure 7). As expected, the mud-rich argillaceous miliolid-skeletal-green algae packstone facies is the poorest reservoir facies because all interparticle pore space was filled by lime mud or terrigenous clays (Fig. 5E). The ooid grainstone facies is the next poorest quality reservoir facies, with very little interparticle porosity retained because of pervasive early cementation by blocky calcite (Fig. 5A), likely caused by an extended period of exposure to a meteoric diagenetic environment (Halley and Harris, 1979; Harris, 1979; Longman, 1980). In contrast, the superficial oolitic-skeletal grainstone and skeletal grainstone facies both retain a significant amount of interparticle pores (Figs. 5B and 5C), and thus are much better reservoir facies. The skeletal grainstone, which most commonly occurs at the base of shoal packages, has the best reservoir quality of the four facies overall (Table 2). These findings corroborate with original core-based studies of the Pettet Formation in Rusk County published by Wiggins and Harris (1984) and Harris and Wiggins (1985).

Facies distribution and stacking patterns across the study area provides insight into the stratigraphic seals affecting hydrocarbon trapping in Pettet Formation reservoirs. Mid-ramp shoal complexes containing the main reservoir facies are sealed updip

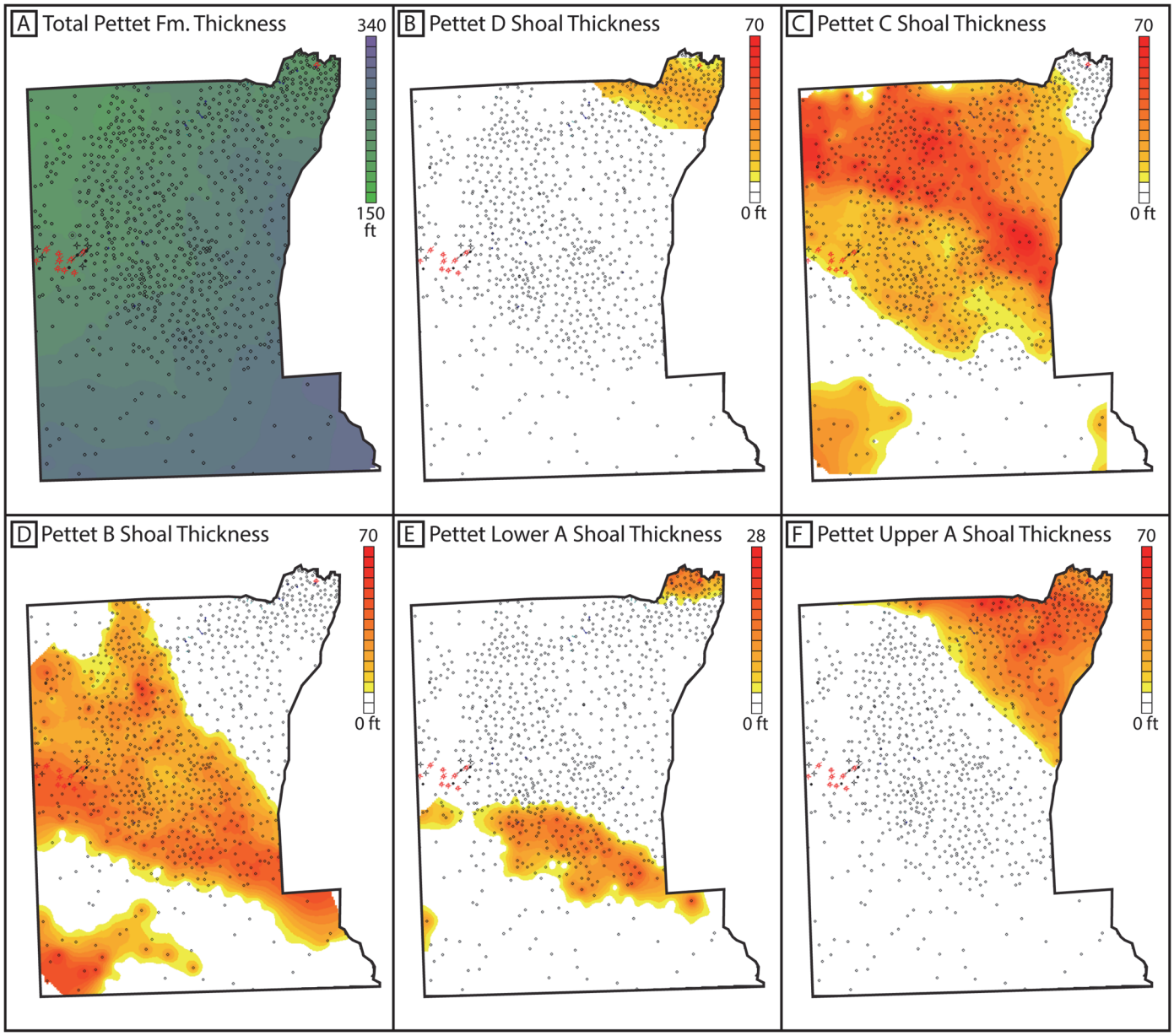

Figure 11. Isopach thickness maps for intervals of the Pettet Formation. (A) Total Pettet Formation thickness. (B) Distribution and total thickness of shoal complex intervals in the Pettet D. (C) Distribution and total thickness of shoal complex intervals in the Pettet C. Note that disconnected shoal occurrence in the southwestern corner of the study area is likely related to presence of shallow-water environments on top of fault blocks in the Mount Enterprise Fault Zone. (D) Distribution and total thickness of shoal complex intervals in the Pettet B. Note continued presence of shoal complexes on Mount Enterprise fault blocks. (E) Distribution and total thickness of shoal complex intervals in the lower Pettet A. This interval captures the major transgressive floodback: shoals in the southwestern half of the study area were deposited in the earliest Pettet A, and shoals in the northeastern half of the study area were deposited in the latest early Pettet A after sea level rise. (F) Distribution and total thickness of shoal complex intervals in the upper Pettet A.

and downdip by tight argillaceous mud-rich facies (argillaceous miliolid-skeletal-green algae packstones, chondrodont-toucasid floatstones, and siliciclastic-rich molluscan packstones) in the inner ramp and middle-outer ramp. They were probably also sealed laterally by similar facies in areas where shoals did not develop in lower energy areas. This facies partitioning across the ramp enabled the same facies group to act as the top and base seal for skeletal and superficial oolitic-skeletal grainstones during progradational sequences. Tight ooid grainstones capping shoal intervals also might have contributed to the stratigraphic top seal.

Understanding the occurrence of stratigraphic seals on reservoir facies of the Pettet Formation is important to understanding the productivity trends of the formation as a whole. Because reservoir facies are constrained to shoal intervals in the Pettet Formation (Fig. 7), and these shoal complexes have been demonstrated to be migratory through time based on eustatic sea-level trends (Figs. 10 and 11), there is a high likelihood of separation of individual shoal bodies. This must be considered when assessing the Pettet Formation for new production, field development, missed-pay, and field extension.

Comparisons to Other Comanche Sections

Past work in the time-equivalent Sligo Formation of South Texas (Bebout, 1977; Bebout et al., 1981) and the San Marcos Arch of Central Texas (Phelps et al., 2014) provide reference sections for comparison of lithofacies of the Pettet Formation. The South and Central Texas studies both report similar low-energy subtidal platform interior facies to those described in this study, largely being composed of variants of argillaceous miliolid-mollusk-calcareous algae-peloid wackestones to packstones with some toucasid, chondrodont, or oyster biostromes. Sand flat/shoal facies are also similar, consisting of a mixture of skeletal (molluscan- and calcareous algae-dominated) and ooid grainstones. However, the facies associated with shoaling cycle caps and transgressive pulses differ between the Central/South Texas region and Rusk County (East Texas).

Comparisons of shoal facies characteristics and cycle capping facies between Sligo and Pettet shoaling cycles suggests a regional variability in the distance between shoreline and shoal facies, possibly driven by local platform architecture and steepness of depositional slope. Cycles in Central and South Texas Sligo sections are commonly capped by laminated microbial mudstone tidal flat facies or anhydrite nodules interpreted to represent a salina-type environment (Bebout, 1977; Bebout et al., 1981; Phelps et al., 2014). Underlying ooid-skeletal grainstone facies exhibit planar or cross-stratified bedding, ripples, and mud drapes, suggesting a shoreline-proximal peritidal depositional environment (Phelps et al., 2014). In contrast, Pettet cycle caps are characterized by well-cemented ooid grainstones, which are rarely planar bedded but more commonly massively bedded and devoid of any mud, terrigenous or carbonate. Tidal flat and/or salina facies are not present. These observations suggest that the Pettet ooid-skeletal grainstone facies were more likely deposited in a mid-ramp shoal environment where shoreline influence was nonexistent. The difference in shoal positioning could possibly be attributed to a greater depositional slope related to differential subsidence in the Central/South Texas region (reduced subsidence rates in proximal settings associated with the Llano Uplift, and greater subsidence in distal settings). Persistent differential subsidence would cause waves to break nearer shore and consequently focus shoal generation there long-term, especially during times of low-amplitude eustatic fluctuations. In contrast, a lower-angle slope in the East Texas/Rusk County region would create a broader shallow-water platform interior and concentrate high wave energy further away from the shoreline. A similar mid-ramp shoal generation effect could be achieved if an underlying subtle topographic high was present to promote wave breakage and subsequent shoal development; however, this is unlikely to be the explanation because shoals in this study are observed migrating across the entire study area instead of remaining concentrated around one location.

Differences in transgressive systems tract facies between the Sligo and Pettet Formations are predominantly related to differing amounts of siliciclastic material. In Central and South Texas, transgressive pulses are associated with a transition to low-energy, carbonate-dominated peloid-skeletal packstones, which may be somewhat argillaceous (Phelps et al., 2014). In East Texas, transgressive facies also become muddier and more peloidal, but differ in the incorporation of a large amount of clay minerals. Larger-scale transgressions are commonly associated with thinly bedded and lenticular rippled mudstone rock fabrics dominated by clay, siliciclastic silt, and oysters. Thus, it appears that the amount of fine particulate terrigenous input is greater in East Texas, promoting more clay-mineral-rich facies in lower-energy areas. Clay and silt materials could be sourced from continental shoreline flooding during transgressions, or they could be reworked and redistributed by currents.

A well-established sequence stratigraphic framework for the Sligo Formation in the San Marcos Arch region provides a useful chronostratigraphic reference that can be tied into this study's investigation of the Pettet Formation. The San Marcos Arch Sligo section preserves four third-order sequences: the Hauterivian–10, Barremian–20, Barremian–30, and Aptian–10 (Phelps et al., 2014). Deposition of the Sligo and Pettet Formations ultimately terminated contemporaneously across the Comanche Platform as a result of effects of OAE1a; the contact with these formations and the overlying siliciclastic-dominated Pine Island Shale thus serves as a reliable point on which to tie the sequence stratigraphic frameworks. Notably, the Pettet Formation only preserves two third-order sequences in comparison to the Sligo Formation's four third-order sequences. We suggest that these two Pettet sequences are correlative to the two latter sequences (Barremian–30 and Aptian–10) documented in the San Marcos Arch Sligo sections. We thus conclude that the transition from a siliciclastic-dominated system (Travis Peak Formation) to a carbonate-dominated system (Pettet Formation) occurred significantly later in the East Texas region than in the San Marcos Arch region. This discrepancy could be attributed to differences in proximity to major siliciclastic sources, or simply to a variation in the amount of terrestrial sediment runoff. Although differences in paleogeography and structural history can be invoked as an alternative driver of the delayed onset of carbonate deposition in East Texas, they are less likely to be primary factors, as the San Marcos Arch represents a structural high with a reduced nearshore subsidence rate related to its attachment to the Llano Uplift (Phelps et al., 2014; Ewing, 2016), and thus should have also had a long period of siliciclastic deposition similar to that of the East Texas study area. Because siliciclastic deposition persisted longer in East Texas, either the study area was uplifting more than the San Marcos Arch (not supported by any structural maps or paleogeographic maps of other formations, e.g., Dutton et al., 1990; Cicero et al., 2010), or volume of siliciclastic input is more likely to have been the main driver.

CONCLUSIONS

This study is the first to establish a robust sequence stratigraphic framework for the Pettet Formation in East Texas. The Pettet Formation is comprised of two third-order composite sequences, which correlate to the Barremian–30 and Aptian–10 sequences delineated in the Sligo Formation by Phelps et al. (2014) in the San Marcos Arch area of central-southern Texas. Initiation of the transgressive portion of the Barremian–30 CS began at the Travis Peak-Pettet contact with the flooding of the Comanche Shelf and establishment of carbonates overlying Travis Peak fluvio-deltaic sediments. During the Barremian–30 highstand, oolitic-skeletal shoal complexes prograded southwest across the study area, punctuated by brief backsteps interpreted to represent fourth-order high-frequency transgressive systems tract floodbacks. A large floodback associated with the Aptian–10 transgression relocated the main carbonate factory far updip to the northeastern corner of the study area before shoal complex progradation resumed in the Aptian–10 highstand.

Facies described in core were divided into three facies associations: (1) high-energy shoal complex; (2) low-energy carbonate-dominated subtidal; and (3) low-energy siliciclastic-dominated subtidal. Mid-ramp shoal complexes, comprised of skeletal grainstones, superficial oolitic-skeletal grainstones, and ooid grainstones, graded laterally into argillaceous low-energy lime mud-dominated ramp interior and middle ramp facies. Low-energy siliciclastic-dominated facies representing the outer ramp environment were only observed in large-scale floodbacks (Aptian–10 transgression). Facies stacking patterns within individual HFS in the regressive portion of CS were found to be remarkably consistent, beginning with facies of the low-energy carbonate-dominated subtidal facies association, then transitioning updip into skeletal grainstones, overlain by superficial oolitic-skeletal grainstones, and finally being capped by

well-cemented ooid grainstones. Because ooid grainstones were deposited in the shallowest water environment and experienced extensive meteoric diagenesis, porosity and permeability values are poor; however, they are an excellent top seal for underlying superficial oolitic-skeletal grainstone and skeletal grainstone reservoirs, which have significantly better interparticle pore preservation and consequently much better reservoir quality.

Mapped occurrence of shoal complexes within each Pettet subunit demonstrates that they developed periodically and prograded significantly across the study area during sea-level highstands, likely related to limitations in accommodation on the very low-angle ramp. The architecture and facies partitioning of the depositional system in the study area is shown to have had significant impact on the stratigraphic and geographic distribution of shoal complexes, which in turn has important implications for reservoir distribution and hydrocarbon production. Connectivity challenges encountered when attempting production from the Pettet Formation may be linked to these isolated discrete shoal bodies, which are stratigraphically sealed laterally by updip and downdip tight mud-rich facies, and vertically by tight ooid grainstones and siliciclastic-rich mudstones.

ACKNOWLEDGMENTS

This study was funded by the State of Texas Advanced Resource Recovery (STARR) Program at the Bureau of Economic Geology, University of Texas at Austin. We are grateful to the staff at the Core Research Center for their assistance in viewing and sampling cores. We also greatly appreciate discussions with Benjamin Smith, which helped improve the manuscript. Reviews by John Griffiths, Michael Vinson, and David Hull were instrumental towards bettering the manuscript into its final form, and we thank them for their insightful comments. Publication authorized by the Director, Bureau of Economic Geology, Jackson School of Geosciences, University of Texas at Austin.

REFERENCES CITED

Bebout, D. G., 1977, Sligo and Hosston depositional patterns, subsurface of South Texas, *in* D. G. Bebout and R. G. Loucks, eds., Cretaceous carbonates of Texas and Mexico: Applications to subsurface exploration: Bureau of Economic Geology Report of Investigations 89, Austin, Texas, p. 79–96.

Bebout, D. G., R. A. Schatzinger, and R. G. Loucks, 1977, Porosity distribution in the Stuart City Trend, Lower Cretaceous, south Texas, *in* D. G. Bebout and R. G. Loucks, eds., Cretaceous carbonates of Texas and Mexico: Applications to subsurface exploration: Bureau of Economic Geology Report of Investigations 89, Austin, Texas, p. 97–126.

Bebout, D. G., D. A. Budd, and R. A. Schatzinger, 1981, Depositional and diagenetic history of the Sligo and Hosston formations (Lower Cretaceous) in South Texas: Bureau of Economic Geology Report of Investigations 109, Austin, Texas, 69 p.

Carozzi, A. V., 1957, *Contribution à l'étude des propriétés géométriques des oolithes*: *L'exemple du Grand Lac Salé*, Utah, USA: *Bulletin de l'Institut National Genevois*, v. 58, p. 3–52.

Cicero, A., I. Steinhoff, T. McClain, K. A. Koepke, and J. D. Dezelle, 2010, Sequence stratigraphy of the Upper Jurassic mixed carbonate/siliciclastic Haynesville and Bossier Shale depositional systems in East Texas and North Louisiana: Gulf Coast Association of Geological Societies Transactions, v. 60, p. 133–148.

Dutton, S. P., S. E. Laubach, R. S. Tye, R. W. Baumgardner, and K. L. Herrington, 1990, Geology of the Lower Cretaceous Travis Peak Formation, East Texas—Depositional history, diagenesis, structure, and reservoir engineering implications: Topical Report prepared by the Bureau of Economic Geology (Austin, Texas) for the Gas Research Institute (Chicago, Illinois) under Contract 5082–211–0708, 183 p.

Ewing, T. E., 2016, Texas through time: Lonestar geology, landscapes, and Resources: Bureau of Economic Geology Udden Series 6, Austin, Texas, 431 p.

Flügel, E., 2010, Microfacies of carbonate rocks: Springer, Heidelberg, Germany, 984 p.

Fritz, D. A., T. W. Belsher, J. M. Medlin, J. L. Stubbs, R. P. Wright, and P. M. Harris, 2000, New exploration concepts for the Edwards and Sligo margins, Cretaceous of onshore Texas: American Association of Petroleum Geologists Bulletin, v. 84, p. 905–922, <http://doi.org/10.1306/A9673B62-1738-11D7-8645000102C1865D>.

Hackley, P. C., and A. W. Karlsen, 2014, Geologic assessment of undiscovered oil and gas resources in Aptian carbonates, onshore northern Gulf of Mexico Basin, United States: Cretaceous Research, v. 48, p. 225–234, <http://doi.org/10.1016/j.cretres.2013.12.005>.

Halley, R. B., and P. M. Harris, 1979, Fresh-water cementation of a 1,000-year-old oolite: Journal of Sedimentary Petrology, v. 49, p. 969–988, <http://doi.org/10.1306/212F7892-2B24-11D7-8648000102C1865D>.

Harris, P. M., 1979, Sedimenta VII: Facies anatomy and diagenesis of a Bahamian ooid shoal: University of Miami, Florida, 163 p.

Harris, P. M., and W. D. Wiggins, 1985, Reservoir potential of shoaling carbonate sequences in the Sligo Formation of East Texas: Gulf Coast Association of Geological Societies Transactions, v. 35, p. 77–79.

Harris, P. M., S. J. Purkis, J. Ellis, P. K. Swart, and J. J. G. Reijmer, 2015, Mapping bathymetry and depositional facies on Great Bahama Bank: Sedimentology, v. 62, p. 566–589, <http://doi.org/10.1111/sed.12159>.

Harris, P. M., M. R. Diaz, and G. P. Eberli, 2019, The formation and distribution of modern ooids on Great Bahama Bank: Annual Review of Marine Science, v. 11, p. 491–516, <http://doi.org/10.1146/annurev-marine-010318-095251>.

Hattori, K. E., R. G. Loucks, and C. Kerans, 2019, Stratal architecture of a halokinetically controlled patch reef complex and implications for reservoir quality: A case study from the Aptian James Limestone in the Fairway Field, East Texas Basin: Sedimentary Geology, v. 387, p. 87–103, <http://doi.org/10.1016/j.sedgeo.2019.04.009>.

Hofling, R., and R. W. Scott, 2002, Early and mid-Cretaceous buildups, *in* W. Kiessling, E. Flügel, and J. Golonca, eds., Phanerozoic reef patterns: Society of Economic Paleontologists and Mineralogists (Society for Sedimentary Geology) Special Publication 72, Tulsa, Oklahoma, p. 521–548, <http://doi.org/10.2110/pec.02.72.0521>.

Hull, D. C., 2011, Stratigraphic architecture, depositional systems, and reservoir characteristics of the Pearsall shale-gas system, Lower Cretaceous, South Texas: M.S. Thesis, University of Texas at Austin, 192 p.

Jackson, M. P. A., and B. D. Wilson, 1982, Fault tectonics of the East Texas Basin (USA).: Bureau of Economic Geology Geological Circular 82–4, Austin, Texas, 31 p.

Jackson, M. P. A., and S. J. Seni, 1983, Geometry and evolution of salt structures in a marginal rift basin of the Gulf of Mexico, East Texas.: Geology, v. 11, p. 131–135, <http://doi.org/10.1130/0091-7613(1983)11<131:GAEOSS>2.0.CO;2>.

Kerans, C., 2002, Styles of rudist buildup development along the northern margin of the Maverick Basin, Pecos River Canyon, southwest Texas: Gulf Coast Association of Geological Societies Transactions, v. 52, p. 501–516.

Kirkland, B. L., R. G. Lighty, R. Rezak, and T. T. Tieh, 1987, Lower Cretaceous barrier reef and outer shelf facies, Sligo Formation, South Texas: Gulf Coast Association of Geological Societies Transactions, v. 37, p. 371–382, <http://doi.org/10.1306/703c7f84-1707-11d7-8645000102c1865d>.

Lobao, J. J., and R. H. J. Pilger, 1984, Early evolution of salt structures in the North Louisiana Salt Basin: Gulf Coast Association of Geological Societies Transactions, v. 35, p. 189–198, <http://doi.org/10.1306/AD462D49-16F7-11D7-8645000102C1865D>.

Longman, M. W., 1980, Carbonate diagenetic textures from nearsurface diagenetic environments: American Association of Petro-

leum Geologists Bulletin, v. 64, p. 461–487, <http://doi.org/10.1306/2F918A63-16CE-11D7-8645000102C1865D>.

Loucks, R. G., 1977, Porosity development and distribution in shoal-water carbonate complexes—Subsurface Pearsall Formation (Lower Cretaceous), South Texas, *in* D. G. Bebout and R. G. Loucks, eds., Cretaceous carbonates of Texas and Mexico: Applications to subsurface exploration: Bureau of Economic Geology Report of Investigations 89, Austin, Texas, p. 97–126.

Loucks, R. G., C. Kerans, H. Zeng, and P. A. Sullivan, 2017, Documentation and characterization of the Lower Cretaceous (Valanginian) Calvin and Winn carbonate shelves and shelf margins, onshore north central Gulf of Mexico: American Association of Petroleum Geologists Bulletin, v. 101, p. 119–142, <http://doi.org/10.1306/06281615248>.

McFarlan Jr., E., and L. S. Menes, 1991, Lower Cretaceous, *in* A. Salvador, ed., The geology of North America, v. J: The Gulf of Mexico Basin: Geological Society of America, Boulder, Colorado, p. 181–204, <http://doi.org/10.1130/DNAG-GNA-J.181>.

Menegatti, A. P., H. Weissert, R. S. Brown, R. V. Tyson, P. Farrimond, A. Strasser, and M. Caron, 1998, High-resolution $\delta^{13}C$ stratigraphy through the Early Aptian "*Livello selli*" of the Alpine Tethys: Paleoceanography and Paleoclimatology, v. 13, p. 530–545, <http://doi.org/10.1029/98PA01793>.

Nichols, J. L., 1958, Sligo stratigraphy of North Louisiana, Arkansas and East Texas, *in* Reference report on certain oil and gas fields: Shreveport Geological Society, p. 1–25.

Nichols, P. H., G. E. Peterson, and C. E. Wuestner, 1968, Summary of subsurface geology of northeast Texas, *in* B. W. Beebe and B. F. Curtis, eds., Natural gases of North America: American Association of Petroleum Geologists Memoir 9, Tulsa, Oklahoma, p. 982–1004, <http://doi.org/10.1306/M9363C69>.

Perkins, B. F., 1974, Paleoecology of a rudist reef complex in the Comanche Cretaceous Glen Rose Limestone of Central Texas: Geoscience and Man, v. 8, p. 131–174.

Phelps, R. M., C. Kerans, R. G. Loucks, R. O. B. P. Da Gama, J. Jeremiah, and D. Hull, 2014, Oceanographic and eustatic control of carbonate platform evolution and sequence stratigraphy on the Cretaceous (Valanginian-Campanian) passive margin, northern Gulf of Mexico: Sedimentology, v. 61, p. 461–496, <http://doi.org/10.1111/sed.12062>.

Phelps, R. M., C. Kerans, R. O. B. P. Da-Gama, J. Jeremiah, D. Hull, and R. G. Loucks, 2015, Response and recovery of the Comanche carbonate platform surrounding multiple Cretaceous oceanic anoxic events, northern Gulf of Mexico: Cretaceous Research, v. 54, p. 117–144, <http://doi.org/10.1016/j.cretres.2014.09.002>.

Reeder, S. L., and E. C. Rankey, 2008, Interactions between tidal flows and ooid shoals, northern Bahamas: Journal of Sedimentary Research, v. 78, p. 175–186, <http://doi.org/10.2110/jsr.2008.020>.

Rogers, R. E., 1968, Carthage Field, Panola County, Texas, *in* B. W. Beebe and B. F. Curtis, eds., Natural gases of North America: American Association of Petroleum Geologists Memoir 9, Tulsa, Oklahoma, p. 1020–1059, <http://doi.org/10.1306/M9363C73>.

Scott, R. W., 1981, Biotic relations in Early Cretaceous coral-algal-rudist reefs, Arizona: Journal of Paleontology, v. 55, p. 463–478.

Shanmugam, G., T. D. Spalding, and D. H. Rofheart, 1993, Process sedimentology and reservoir quality of deep-marine bottom-current reworked sands (sandy contourites): An example from the Gulf of Mexico: American Association of Petroleum Geologists Bulletin, v. 77, p. 1241–1259, <http://doi.org/10.1306/BDFF8E52-1718-11D7-8645000102C1865D>.

Shanmugam, G., 2000, 49 years of the turbidite paradigm (1950s-1990s): Deep-water processes and facies models—A critical perspective: Marine and Petroleum Geology, v. 17, p. 285–342, <http://doi.org/10.1016/S0264-8172(99)00011-2>.

Sitgreaves, J. R., 2015, Shelf-to-basin architecture and facies variability of a Cretaceous intrashelf basin in the northwest Gulf of Mexico: M.S. Thesis, University of Texas at Austin, 77 p.

Spears, C. S., 2020, Analysis of the depositional systems, lithofacies, diagenesis, and reservoir quality of the Lower Cretaceous Pettet Limestone reservoir section of the Wright Mountain Field in the East Texas Basin: M.S. Thesis, University of Texas at Austin, 88 p.

Strasser, A., 1986, Ooids in Purbeck limestones (lowermost Cretaceous) of the Swiss and French Jura: Sedimentology, v. 33, p. 711–727, <http://doi.org/10.1111/j.1365-3091.1986.tb01971.x>.

Walker, J. D., J. W. Geissman, S. A. Bowring, and L. E. Babcock, 2018, Geologic time scale, v. 5.0: Geological Society of America, <http://doi.org/10.1130/2018.CTS005R3C>.

Weissert, H., and E. Erba, 2004, Volcanism, CO_2 and palaeoclimate: A late Jurassic–early Cretaceous carbon and oxygen isotope record: Journal of the Geological Society, v. 161, p. 695–702, <http://doi.org/10.1144/0016-764903-087>.

Wiggins, W. D., and P. M. Harris, 1984, Cementation and porosimetry of shoaling sequences in the subsurface Pettit Limestone, Cretaceous of East Texas, *in* P. M. Harris, ed., Carbonate sands—A core workshop: Society of Economic Paleontologists and Mineralogists, Tulsa, Oklahoma, p. 263–305, <http://doi.org/10.2110/cor.84. 05.0263>.

Wissler, L., H. Funk, and H. Weissert, 2003, Response of Early Cretaceous carbonate platforms to changes in atmospheric carbon dioxide levels: Palaeogeography, Palaeoclimatology, Palaeoecology, v. 200, p. 187–205, <http://doi.org/10.1016/S0031-0182(03)00450-4>.